RESEARCH PAPER

A photoswitchable GABA receptor channel blocker

Galyna Maleeva[1] | Daniel Wutz[2] | Karin Rustler[2] | Alba Nin-Hill[3] | Carme Rovira[3,10] |
Elena Petukhova[6] | Antoni Bautista-Barrufet[7] | Alexandre Gomila-Juaneda[7] |
Petra Scholze[8] | Franck Peiretti[9] | Mercedes Alfonso-Prieto[4,5] | Burkhard König[2] |
Pau Gorostiza[7,10,11] | Piotr Bregestovski[1,6,12]

[1] INSERM, INS, Institut de Neurosciences des Systèmes, Aix-Marseille University, Marseille, France

[2] Institute of Organic Chemistry, University of Regensburg, Regensburg, Germany

[3] Departament de Química Inorgànica i Orgànica (Secció de Química Orgànica) and Institut de Química Teòrica i Computacional (IQTCUB), Universitat de Barcelona, Barcelona, Spain

[4] Department of Computational Biomedicine, Institute for Advanced Simulations IAS-5 and Institute of Neuroscience and Medicine INM-9, Forschungszentrum Jülich GmbH, Jülich, Germany

[5] Cécile and Oskar Vogt Institute for Brain Research, Medical Faculty, Heinrich Heine University Düsseldorf, Düsseldorf, Germany

[6] Department of Normal Physiology, Kazan State Medical University, Kazan, Russia

[7] Institute for Bioengineering of Catalonia (IBEC), The Barcelona Institute of Science and Technology (BIST), Barcelona, Spain

[8] Department of Pathobiology of the Nervous System, Center for Brain Research, Medical University Vienna, Vienna, Austria

[9] INSERM 1263, INRA 1260, C2VN, Aix-Marseille Université, Marseille, France

[10] Institució Catalana de Recerca i Estudis Avançats (ICREA), Barcelona, Spain

[11] Network Biomedical Research Center in Biomaterials, Bioengineering and Nanomedicine (CIBER-BBN), Spain

[12] Institute of Neurosciences, Kazan State Medical University, Kazan, Russia

Correspondence
Piotr Bregestovski, INSERM, INS, Institut de Neurosciences des Systèmes, Aix-Marseille University, 13005 Marseille, France.
Email: piotr.bregestovski@univ-amu.fr; pbreges@gmail.com

Mercedes Alfonso-Prieto, Department of Computational Biomedicine, Institute for Advanced Simulations IAS-5 and Institute of Neuroscience and Medicine INM-9, Forschungszentrum Jülich GmbH, D-52425 Jülich, Germany.
Email: malfonsoprieto@gmail.com

Pau Gorostiza, Institute for Bioengineering of Catalonia (IBEC), The Barcelona Institute of Science and Technology (BIST), Barcelona, Spain.
Email: pau@icrea.cat

Background and Purpose: Anion-selective Cys-loop receptors (GABA and glycine receptors) provide the main inhibitory drive in the CNS. Both types of receptor operate via chloride-selective ion channels, though with different kinetics, pharmacological profiles, and localization. Disequilibrium in their function leads to a variety of disorders, which are often treated with allosteric modulators. The few available GABA and glycine receptor channel blockers effectively suppress inhibitory currents in neurons, but their systemic administration is highly toxic. With the aim of developing an efficient light-controllable modulator of GABA receptors, we constructed azobenzene-nitrazepam (Azo-NZ1), which is composed of a nitrazepam moiety merged to an azobenzene photoisomerizable group.

Experimental Approach: The experiments were carried out on cultured cells expressing Cys-loop receptors of known subunit composition and in brain slices using patch-clamp. Site-directed mutagenesis and molecular modelling approaches were applied to evaluate the mechanism of action of Azo-NZ1.

Key Results: At visible light, being in *trans*-configuration, Azo-NZ1 blocked heteromeric α1/β2/γ2 GABA$_A$ receptors, ρ2 GABA$_A$ (GABA$_C$), and α2 glycine receptors, whereas switching the compound into *cis*-state by UV illumination restored the activity. Azo-NZ1 successfully photomodulated GABAergic currents recorded from dentate gyrus neurons. We demonstrated that in *trans*-configuration, Azo-NZ1 blocks the Cl-selective ion pore of GABA receptors interacting mainly with the 2′ level of the TM2 region.

Conclusions and Implications: Azo-NZ1 is a soluble light-driven Cl-channel blocker, which allows photo-modulation of the activity induced by anion-selective Cys-loop receptors. Azo-NZ1 is able to control GABAergic postsynaptic currents and provides new opportunities to study inhibitory neurotransmission using patterned illumination.

1 | INTRODUCTION

The major inhibitory neurotransmission in the mammalian CNS is provided by GABA$_A$, GABA$_A$ ρ (also known as GABA$_C$ ρ receptor; see Alexander et al., 2015), and glycine receptors (Langosch, Becker, & Betz, 1990). In different combinations, these receptors are widely expressed throughout the nervous system and are involved in physiological functions such as cognition, learning, memory, and motor control. Disequilibrium in the functioning of GABA and glycine (Gly) receptors leads to important disorders including epilepsy, anxiety, depression, misbalance of blood pressure, sleep disorders, schizophrenia, and hyperekplexia (Johnston, Chebib, Hanrahan, & Mewett, 2003; Tan, Rudolph, & Lüscher, 2011; Sieghart, 2015; Lynch, 2004).

The activity of GABA$_A$ receptors can be successfully regulated with allosteric modulators like benzodiazepines, including flumazenil and diazepam. They are among the most popular pharmacological drugs and are commonly prescribed to treat insomnia, anxiety, and convulsions. Benzodiazepines can potentiate GABA receptors through interaction with different sites in the receptor displaying nano- and micromolar affinities (Sieghart, 2015). Therefore, benzodiazepine derivatives are convenient scaffolds to develop new modulators of GABA receptor function.

Light-switchable ligands have become a useful tool to specifically control ionic channels, cellular functions, the activity of neuronal circuits, and behaviour (Gorostiza & Isacoff, 2008; Kramer, Mourot, & Adesnik, 2013). The pharmacological activity of ligands can be regulated with photochromic groups—molecules that change their configuration upon illumination with different wavelengths. Azobenzene undergoes a rapid *trans–cis* photoisomerization and has been widely used for this purpose. In the dark, or under visible light irradiation, azobenzene is in the elongated *trans*-configuration, while upon illumination with UV light (360–380 nm), it isomerizes to its *cis*-state and becomes shorter by several angstroms (Gorostiza & Isacoff, 2008; Yu & Ikeda, 2004).

With the aim of regulating the activity of GABA receptors with light, we constructed a series of azobenzene derivatives of nitrazepam and

What is already known

- Pharmacological activity of ligands can be regulated with azobenzene photochromic group, which changes its configuration upon illumination with light of different wavelength.

What this study adds

- Azobenzene-nitrazepam based photochromic compound Azo-NZ1 is a light controllable channel blocker of heteromeric GABA$_A$, homomeric GABA$_C$ ρ2 receptors, and α2 GlyRs.
- Azo-NZ1 modulates in a light-dependent manner synaptic GABAergic currents in dentate gyrus of hippocampal brain slices.

What is the clinical significance

- Azo-NZ1 modulates in a light-dependent manner synaptic GABAergic currents in dentate gyrus of hippocampal brain slices.

characterized their properties. Herein, we describe the interaction of one of these compounds, azobenzene-nitrazepam-1 (Azo-NZ1), with several subtypes of anion-selective Cys-loop receptors (GABA$_A$, GABA$_C$ and glycine receptors). Azo-NZ1 successfully photocontrolled GABAergic currents in cultured cells and in brain slices, but in contrast to the intended design to obtain an allosteric ligand of the classical diazepam site, we found that the azobenzene sulfonyl group introduced alters the binding properties of the compound, enabling light-controlled blocking of the chloride-selective ion pore. Thus, Azo-NZ1 reveals a class of photochromic ligand with a structure capable of blocking the anion-selective channel pore of several Cys-loop receptors.

2 | METHODS

2.1 | Synthesis of compounds

7-Aminonitrazepam (Guandalini et al., 2008; Severino et al., 2008) and tetrabutylammonium 4-nitrosobenzenesulfonate (Priewisch & Rück-Braun, 2005) were synthesized according to previously reported procedures. Commercial reagents and starting materials were purchased from Acros Organics, Alfa-Aesar, Fisher Scientific, Sigma Aldrich, or VWR and used without any further purification. Solvents used were of p.a. quality and dried according to common procedures, if necessary. Commercially obtained phosphate buffer (pH = 7.4) was used for investigations of the photochromic properties. Dry nitrogen was used as inert gas atmosphere. A Biotage Isolera flash purification system with UV/Vis detector using Sigma Aldrich MN silica gel 60 M (40–63 μm, 230–400 mesh) for normal phase or pre-packed Biotage SNAP cartridges (KP C18 HS) for reversed phase chromatography was used for automated flash column chromatography. Reaction monitoring via TLC and determination of R_f values was accomplished on alumina plates coated with silica gel (Merck silica gel 60 F254, 0.2 mm). Melting points were measured with a Stanford Research Systems OptiMelt MPA 100 device and are uncorrected. NMR spectra were measured on Bruker Avance 300 (^{1}H 300.13 MHz, ^{13}C 75.48 MHz), Bruker Avance 400 (^{1}H 400.13 MHz, ^{13}C 100.61 MHz), and Bruker Avance III 600 (^{1}H 600.25 MHz, ^{13}C 150.95 MHz) instruments. The spectra are referenced against the NMR solvent (DMSO-d_6: δ_H = 2.50 ppm), and chemical shifts, δ, are reported in ppm. Resonance multiplicity is abbreviated as follows: s (singlet), d (doublet), t (triplet), q (quartet), m (multiplet), and b (broad). Carbon NMR signals are reported using DEPT 135 and ^{1}H–^{13}C HSQC spectra with (+) for primary/tertiary, (−) for secondary, and (q) for quaternary carbons. An Agilent Q-TOF 6540 UHD (ESI–MS) instrument was used for recording mass spectra. UV/Vis absorption spectroscopy was accomplished using a Varian Cary BIO 50 UV/Vis spectrometer in 10-mm quartz cuvettes. IR spectra were recorded on an Agilent Cary 630 FT-IR spectrometer, and the peak positions are reported in wavenumbers (cm^{-1}). Analytical HPLC measurements were performed on an Agilent 1220 Infinity LC (column: Phenomenex Luna 3 μM C18(2) 100 Å, 150 × 2.00 mm; flow: 0.3 ml·min^{-1} at 30°C; solvent A: MilliQ water with 0.05% vol TFA; solvent B: MeCN). The ratios in the photostationary states (PSSs) were determined by HPLC measurements with a detection wavelength at the isosbestic points. For determination of the thermal half-lives, the solutions were irradiated until the photostationary state was reached. Then the solutions were left at 25°C, and the recovery of the absorbance of the *trans*-isomer at λ_{max} was measured. Consequently, the thermal half-life was calculated by fitting the data with a single exponential function. An Agilent 1260 system (column: Phenomenex Luna 10 μM C18(2) 100 Å, 250 × 21.2 mm; flow: 22.0 ml·min^{-1}; solvent A: MilliQ water with 0.05% vol TFA; solvent B: MeCN) was used for preparative HPLC purification. Light sources for irradiation: λ = 365 nm (Herolab handheld lamp UV-6 L, 6 W), λ = 455 nm (OSRAM Oslon SSL 80 LED, 700 mA, 1.12 W). The power of the light is given based on the specifications supplied by the company when the lamps were purchased. Final compounds for biological testing possess a purity ≥95%, as determined by HPLC measurements with detection at 220 and 254 nm.

Azo-NZ1 ((*E*)-4-((2-oxo-5-phenyl-2,3-dihydro-1*H*-benzo[*e*][1,4] diazepin-7-yl)diazenyl)benzenesulfonic acid) was synthesized according to the following procedure (Figure 1b). Tetrabutylammonium 4-nitrosobenzenesulfonate (236 mg, 0.54 mmol, 1.0 eq.) was added to a solution of 7-aminonitrazepam (68 mg, 0.27 mmol, 1.0 eq.) in acetic acid (2 ml) and CH$_2$Cl$_2$ (1 ml). After the mixture had been stirred for 24 hr at room temperature, the solvent was removed in vacuo.
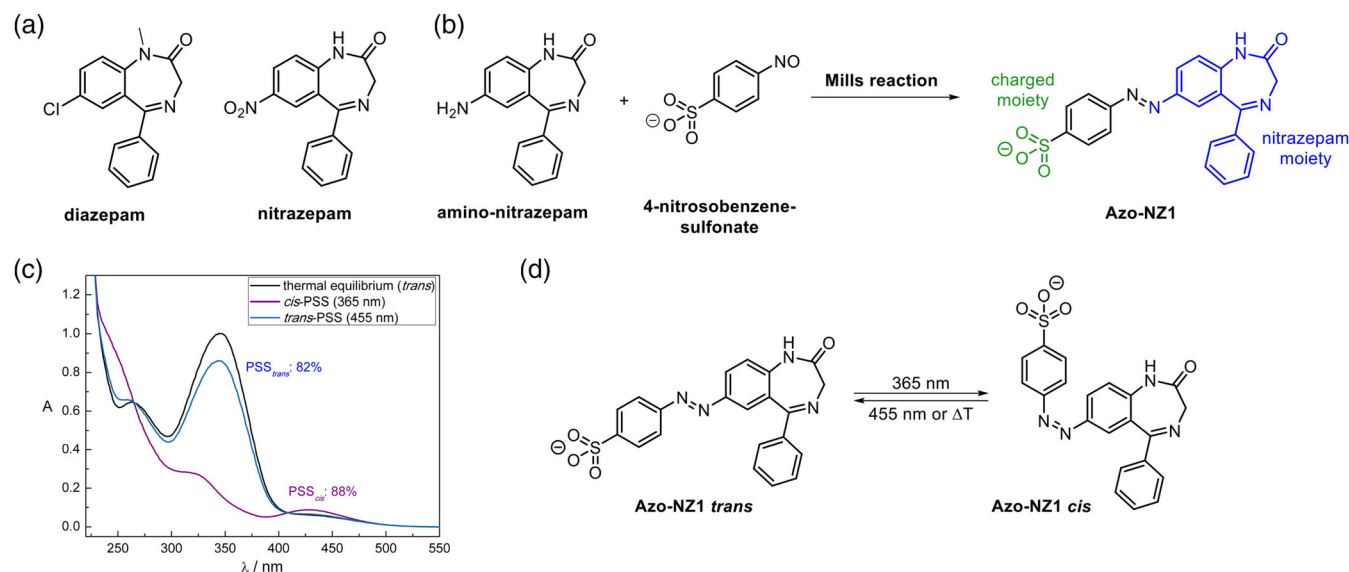
FIGURE 1 Design of Azo-NZ1. (a) Chemical formula of diazepam and nitrazepam. (b) Synthetic approach for the synthesis of Azo-NZ1. (c) UV–Vis spectra of azo-nitrazepam Azo-NZ1 (50 μM in phosphate buffer +0.1% DMSO) from the *trans*-isomer (black), the PSS at irradiation with UV light of λ = 365 nm (purple), and the PSS at irradiation with blue light of λ = 455 nm (blue). (d) Schematic representation of Azo-NZ1 in its *trans*- and *cis*-configurations

Purification by automated flash column chromatography (CH_2Cl_2/MeOH, 3–25% MeOH) and subsequent preparative HPLC (2–65% MeCN in 10 min, t_R = 7.2 min) yielded Azo-NZ1 (69 mg, 61%) as a yellow solid. R_f 0.03 (CH_2Cl_2/MeOH 9:1); mp 280°C (decomposition); ^{1}H-NMR (600 MHz, DMSO-d_6) δ = 11.32 (s, 1H), 8.23 (dd, J = 8.8, 2.4 Hz, 1H), 7.81–7.78 (m, 2H), 7.77–7.73 (m, 3H), 7.68 (t, J = 7.4 Hz, 1H), 7.64 (dd, J = 8.3, 1.3 Hz, 2H), 7.57 (t, J = 7.7 Hz, 2H), 7.52 (d, J = 8.9 Hz, 1H), 4.34 (s, 2H); ^{13}C-NMR (151 MHz, DMSO-d_6) δ = 172.5 (q), 168.9 (q), 151.4 (q), 151.1 (q), 146.5 (q), 143.0 (q), 135.8 (q), 132.5 (+), 130.7 (+), 128.8 (+), 128.6 (+), 126.8 (+), 126.2 (+), 124.4 (q), 122.9 (+), 122.2 (+), 54.6 (−); IR (neat) ν = 3489, 3135, 2930, 1715, 1614, 1484, 1435, 1387, 1342, 1230, 1163, 1115, 1029, 1006, 846, 742, 697 cm^{-1}; HRMS (ESI) calculated for $C_{22}H_{16}N_4O_4S$ $(M + H)^+$ m/z = 421.0965; found 421.0964.

2.2 | Cell culture and transfection

The experiments were carried out on cultured CHO cells (CHO-K1, ATCC Cat# CCL-61, RRID:CVCL_0214) obtained from the American Type Tissue Culture Collection (ATCC, Molsheim, France) that were maintained in culture conditions as previously described (Maleeva, Peiretti, Zhorov, & Bregestovski, 2017; Mukhtarov et al., 2013). For electrophysiological analysis, cells were transfected with cDNAs of several Cys-loop receptors. For expression of heteromeric $GABA_A$ receptors, cells were simultaneously transfected with cDNA (concentrations 0.9–1.2 µg·µl^{-1}) of α1, β2, and γ2 (isoform S) subunits. For expression of homomeric $GABA_C$ receptors, cells were transfected with cDNA of ρ1 or ρ2 subunits. For the expression of homomeric glycine receptors and 5-HT3A receptors, cDNAs of α1, α2, and A subunits, respectively, were used.

One day before transfection, cells were plated on the cover slips (12 mm in diameter) and placed inside 35-mm cell culture dishes with 2 ml of medium. Transfection was performed using the Lipofectamine 3000 protocol (Life Technology, USA). To facilitate identification of transfected cells, a GFP (0.5 µg·µl^{-1}) was added to the transfection mixture. Electrophysiological recordings were performed in the fluorescent cells 24–72 hr after transfection.

2.3 | Electrophysiological recordings on CHO cells

Whole-cell recordings were performed at room temperature (20–25°C) using an EPC-9 amplifier (HEKA Elektronik, Germany). Cells were continuously superfused with external solution containing (mM): NaCl 140, $CaCl_2$ 2, KCl 2.8, $MgCl_2$ 4, HEPES 20, glucose 10; pH 7.4; 320–330 mOsm. Intracellular solution used for filling recording patch pipettes contained (mM): KCl 140, $MgCl_2$ 2, MgATP 2, HEPES10, BAPTA (tetrapotassium salt) 2; pH 7.3; 290 mOsm.

Recording pipettes were pulled from borosilicate glass capillaries (Harvard Apparatus Ltd, USA) and had resistances of 5–10 MOhms. For the rapid replacement of the solutions, the fast application system was used. Three parallel rectangular tubes (100 × 100 µm) were positioned 40–50 µm above the recorded cell. The movement of the tubes was controlled by a computer-driven fast exchange system (SF 77A Perfusion Fast-Step, Warner, USA) allowing a 10–90% solution

exchange in 3–5 ms, as measured by open electrode controls (1/10 external solution/water). Cells with a low input resistance (<150 MOhms) and a rapid run-down (>30% with repetitive application) were excluded from analysis.

The effect of Azo-NZ1 was examined either using a "long" protocol for application of solutions, at constant holding membrane potentials (V_h) of +30 and −30 mV or using a "ramp" protocol that allowed a linear change of membrane potential from −60 to +60 mV (see Figure 3 c). For $GABA_C$ ρ2, ρ1 P2′S, and α2 glycine receptors, the controls correspond to the amplitude of the current just before application of Azo-NZ1, whereas for $GABA_A$ receptors, the control corresponds to the amplitude of the current at wash-out, due to the desensitization of this type of receptor.

UV (365 nm) LED (Thorlabs) was placed at the distance of 4–5 cm from the cell that was being recoreded. The power of UV light was reaching 0.6 mW·mm^{-2} at the level of recording chamber, as determined using an optical power metre (Thorlabs).

2.4 | Electrophysiological recording on brain slices and electrical stimulation

Experiments were performed on white laboratory ICR outbred mice of both genders, kept at 12 hr "day"/"night" cycle. Other details are described previously (Petukhova, Ponomareva, Mukhamedyarov, Maleeva, & Bregestovski, 2018). All animal protocols and experimental procedures were approved by the Local Ethics Committee of Kazan State Medical University (N742.13.11.84 and N1045-72) and by the INSERM Ethics Committee for Animal Experimentation (#30-03102012). Animal studies are reported in compliance with the ARRIVE guidelines (Kilkenny et al., 2010) and with the recommendations made by the British Journal of Pharmacology.

Coronal slices, containing hippocampus, were obtained from 3- to 4-week-old mice. Animals were decapitated under isoflurane anaesthesia. Whole brains were rapidly removed from the skull and immersed for 10 min in ice-cold artificial CSF (aCSF) solution containing (in mM): NaCl 126, KCl 3.5, $CaCl_2$ 2, $MgCl_2$ 1.3, $NaHPO_4$ 1.2, glucose 10, $NaHCO_3$ 25 (pH 7.3–7.4, 290–300 mOsm). The aCSF was continuously oxygenated with 95% O_2 and 5% CO_2 to maintain the physiological pH. Sagittal slices (350 mm) were cut using a tissue slicer (Microm International, Germany) in high K^+ solution, containing (in mM): Kgluconate 120, HEPES-acid 10, Nagluconate 15, EGTA 0.2, NaCl 4 (pH 7.2, 290–300 mOsm). After being cut, slices were placed for 15 min at room temperature in a choline-based solution, containing (in mM): choline chloride 110, KCl 2.5, NaH_2PO_4 1.25, $MgCl_2$ 10, $CaCl_2$ 0.5, $NaHCO_3$ 25, glucose 10, sodium pyruvate 5 (pH 7.3–7.4, 290–300 mOsm). Then, slices were placed in a chamber filled with oxygenated aCSF. Before use, slices were allowed to recover for at least 1 hr at room temperature. Experiments were performed during the period of 1–6 hr after slicing.

During the recordings, slices were placed in a conventional chamber superfused with aCSF (32–34°C). The inhibitory postsynaptic currents evoked (eIPSCs) were recorded from granule cells of dentate gyrus using the patch-clamp technique in whole-cell configuration at −70 or 0 mV. Patch electrodes were pulled from borosilicate capillary

glass (Sutter Instruments flaming/brown micropipette puller P-97) and filled with intracellular solution containing (in mM): Kgluconate 120, KCl 20, $MgCl_2$ 2, MgATP 2, HEPES/KOH 10, BAPTA 1; pH 7.3; 290 mOsm. The resistance of electrodes used was 5–7 MΩ. Membrane currents were recorded at 3–10 kHz using an EPC-9 patch-clamp amplifier (HEKA Elektronik, Germany).

In granule cells of dentate gyrus, postsynaptic currents consist of two main populations: glutamatergic and GABAergic. In our experimental conditions, the reversal potentials for glutamate- and GABA-induced currents were about 0 and −50 mV, respectively. To isolate GABAergic synaptic events from glutamatergic ones without using specific pharmacological antagonists, we performed analysis of Azo-NZ1 action on eIPSCs at V_h = 0 mV. At this potential, glutamatergic events are not detectable, and GABAergic currents appear as outwardly directed deflections. An application of bicuculline at the end of recordings resulted in the complete suppression of these currents, ensuring its pure GABAergic nature.

For the induction of GABAergic responses, stimulation pulses were generated by the DS3 Constant Current Isolated Stimulator (Digitimer, England). Pulses were delivered every 10 s at V_h = 0 mV, the amplitudes of control eIPSCs ranged from 50 to 400 pA. Electrodes for stimulation were prepared from double-barrelled borosilicate theta-tubes (OD = 1.5 mm, ID = 1.0 mm, septum = 0.2 mm, from Warner Instruments, USA). They were pulled using the programme similar to those for preparing patch-clamp recording pipettes, polished, and backfilled with aCSF. To deliver an electrical stimulus, two fine silver wires were inserted into the theta-glass.

After a whole-cell configuration had been obtained with a neuron, the stimulation electrode was placed on the granule cell layer in close proximity within the recording cell (distance 100–200 μm) located towards the hilar region. This allowed the stimulation of presynaptic fibres from the presumed GABAergic basket cells, as described by others (Haselmann, Röpke, Werner, Kunze, & Geis, 2015; Korshoej, Holm, Jensen, & Lambert, 2010).

Previous studies demonstrated that azobenzene-based UV-controlled molecules might be successfully used in living tissues for research purposes (Lin et al., 2015; Yue et al., 2012). However, after prolonged exposure, UV and near-UV irradiation can be damaging (Kienzler et al., 2013). To avoid direct illumination of brain slices with UV light, which might modify synaptic function, we illuminated the aCSF with diodes emitting either UV (365 nm) or blue (455 nm) light. The speed of the perfusion was about 20 ml·min^{-1}, and it was taking 18-20 s for the illuminated solution to arrive to the experimental chamber.

Effects of Azo-NZ1 on the amplitudes of eIPSCs were studied using the following protocol: 20–30 eIPSCs were recorded in control condition, then slices were incubated in aCSF + Azo-NZ1 for 5–10 min at visible or blue (455 nm) light (the compound in *trans*-configuration); the aCSF + Azo-DZ1 was illuminated with UV light for 3–5 min (switching the compound into *cis*-configuration); and subsequently illuminated for 3–5 min with blue light. Changes in UV/blue light illumination could be repeated several times on the same neuron before it is washed with control aCSF. Control tests showed that UV illumination of the pure aCSF for 5 min had no effect on eIPSCs.

2.5 | Data and statistical analysis

The data and statistical analysis comply with the recommendations on experimental design and analysis in pharmacology. Electrophysiological recordings were performed using PatchMaster (HEKA Electronic, Germany) software. To plot concentration–response curves, responses to different concentrations of GABA were fitted using a non-linear fitting routine of the Origin 7.5 software (OriginLabs, USA) with the Hill equation:

$$I = I_{max}/(1 + (EC_{50}/[A])^{n_H}),$$

where I is the normalized current amplitude induced by the agonist at concentration $[A]$, I_{max} is a maximal current induced at given cell, n_H is the Hill coefficient, and EC_{50} is the concentration at which a half-maximum response was induced.

Ionic current recordings were analysed with Igor Pro 6.02 and Origin 9.0 software. In some cases, data were normalized to perform a comparison between different types of receptor or different agonist concentrations. Data are presented as means ± SEM. Significance of difference was evaluated by using two-sample t test, paired sample Wilcoxon signed rank test, and Mann–Whitney U test. Differences were considered significant at a value of P below .05.

2.6 | Materials

All the drugs were obtained from Tocris or Sigma–Aldrich (France). Stock solutions of Azo-NZ1 (10 mM) and diazepam (50 mM) were prepared using DMSO and then diluted to the final concentration in extracellular solution. Stock solutions of GABA (1 M), glycine (1 M), 5-HT (10 mM), APV (40 mM), and bicuculline (10 mM) were prepared using MilliQ water.

2.7 | Modelling

Five different GABA receptor structures were used, all corresponding to open channel states. For $GABA_A$ receptors, we used the homology model of the heteropentameric α1/β2/γ2 receptor from reference (Bergmann, Kongsbak, Sørensen, Sander, & Balle, 2013). Two homology models were generated for the ρ1 and ρ2 $GABA_A$ ($GABA_C$) receptors, using as a template the GluCl receptor in the open channel state (PDB code 3RI5; Hibbs & Gouaux, 2011) and the Swiss-Model server (Biasini et al., 2014). The sequence identity between the GluCl template and the ρ1 and ρ2 receptors is 37% and 36.6%, and it is even higher when only the pore-lining helices are considered (54.2% and 58.3%, respectively). Indeed, GluCl has been proposed to be the best template to model the structure of $GABA_A$ ρ receptors (Naffaa, Chebib, Hibbs, & Hanrahan, 2015). For the S2′G ρ1 and P2′S ρ2 mutant receptors, the mutation was introduced in silico using the Molefacture tool (version 1.3) in VMD (version 1.9.2; Humphrey, Dalke, & Schulten, 1996).

While this manuscript was under review, new cryo-electron microscopy structures of $GABA_A$ receptors were published (Laverty et al., 2019; Masiulis et al., 2019). These structures correspond to either closed or desensitized states of the receptor and hence were not used

for our docking analysis Nonetheless, we superimposed the structural model of the open state used here (Bergmann, Kongsbak, Sørensen, Sander, & Balle, 2013) with the cryo-EM structures of GABA$_A$ receptor in the closed and desensitized states (Figure S9), in order to investigate the possibility of Azo-NZ1 binding to these other two pore conformations. In the closed state, the pore is narrower than in the open state (Figure S9A,B) and thus would hinder binding of the longer and bulkier *trans*-Azo-NZ1, compared to the smaller pore blocker picrotoxinin captured in the cryo-EM structure. For the desensitized state, the pore size is not as different from the open state (Figure S9B,C), and thus, we cannot exclude binding of *trans*-Azo-NZ1. However, we speculate that the non-chloride-conductive desensitized state might be less suitable to bind the chloride-mimic sulphonate group of *trans*-Azo-NZ1. In addition, binding of *trans*-Azo-NZ1 to Ser2′ could prevent desensitization, similarly to picrotoxinin (Gielen, Thomas, & Smart, 2015) and thus would be incompatible with a desensitized state.

2.7.1 | Azo-NZ1 ligand

The initial structures of the Azo-NZ1 compound (*cis*- and *trans*-isomers) were created employing Avogadro (version 1.1.1; Hanwell et al., 2012). For each isomer, two 1,4-diazepine ring conformations, M and P, were considered, which differ in orientation (below or above the plane, respectively) of C3 and the phenyl substituent of C5 (Figure S10). For classical benzodiazepines that bind to the canonical allosteric site, the M conformation is the bioactive one (i.e., with higher affinity for receptor; Richter et al., 2012). However, it is not known a priori whether Azo-NZ1 would exhibit similar conformational preferences, since it binds in a distinct site. Therefore, all four ligand structures (cis/M, cis/P, trans/M, and trans/P) were optimized using quantum mechanical calculations in order to (a) optimize the manually built ligand structures and (b) estimate the relative stability of the M and P conformers. Calculations were performed with the Gaussian 09 (G09) programme package (Frisch et al., 2013), using density functional theory (Rajagopal & Callaway, 1973), with the B3LYP functional (Stephens, Devlin, Chabalowski, & Frisch, 1994) and the 6–31++G(d,p) basis set. For the *trans*-isomer, the two conformers differ only by 0.03 kcal·mol^{-1}, and thus, their Boltzmann populations are very similar (51.4% and 48.6% for P and M, respectively). In other words, the two conformers can be present at room temperature. In the case of the *cis*-isomer, the P conformer is significantly more stable (by 3.5 kcal·mol^{-1}) than the M one, and thus, it is the predominant conformer (with a Boltzmann population of 99.7%).

2.7.2 | Docking calculations

Autodock Vina (version 1.1.2; Trott & Olson, 2010) was employed for ligand–receptor docking. Given that experimental data indicate that Azo-NZ1 binds inside the pore, we centred our search space around the M2 helixes of the pore. A flexible docking approach was used, in which both the receptor and the ligand were considered as flexible. On the one hand, the ligand was allowed to change its geometry (by exploring all the possible ligand torsions) in order to optimize its fit inside the pore. On the other hand, the side chains of the pore-lining residues at positions 2′, 6′, 9′, 13′, and 16′ were allowed to move and adapt to the ligand poses. The maximum energy difference between the best and worst binding modes and the exhaustiveness were set to default values (3 and 8 kcal·mol^{-1}, respectively). Instead, the maximum number of modes was increase to 20 in order to increase the docking sampling. This protocol was repeated 10 times [for GABA$_A$ ρ (GABA$_C$) receptors] and eight times (for GABA$_A$ receptors), starting with different random seeds, so that a total number of 200 and 160 binding modes was obtained for each of the four possible conformers of azo-NZ1 (200 for *cis*/M and *cis*/P, and 160 for *trans*/M and *trans*/P). The docking poses of each conformer were analysed separately. For simplicity, only the *trans*/P and *cis*/P results are discussed in the main text. The results of the corresponding M conformers are almost identical (and in the case of *cis*/M, it has very low population).

We would like to note here that, upon UV light irradiation, *cis*-Azo-NZ1 may either remain in the channel (assuming another binding conformation that unblocks the pore) or exit the pore (reaching the bath solution). The outcome will depend on the mean open time of the channel and the dissociation rate of *cis*-Azo-NZ1. Unfortunately, the dissociation rate is particularly difficult to study either experimentally or computationally. Nevertheless, we expected it to be slow, based on the observations for GABA$_A$ receptors with another pore blocker picrotoxinin (Gielen, Thomas, & Smart, 2015; Korshoej, Holm, Jensen, & Lambert, 2010). Therefore, since with the data at hand we cannot distinguish between the two possibilities put forward above, we decided to perform docking calculations not only with *trans*-Azo-NZ1 but also with the *cis*-isomer, in order to model the situation immediately after UV irradiation. These dockings are aimed at investigating the change in the receptor–ligand binding mode upon *trans–cis* isomerization (both in terms of position along the pore and interactions with the pore-lining residues).

2.7.3 | Analysis of the docking results

We used two different approaches to pinpoint the exact binding site of Azo-NZ1. The first approach was to use the number density of the sulfonate group to follow ligand binding. Previous studies have successfully used this type of analysis to identify ligand binding sites in other ion channels (Raju, Barber, LeBard, Klein, & Carnevale, 2013). The underlying assumption is that regions of continuous density (or high occupancy) should represent regions of tighter binding. We computed the number density value, using the Volmap plugin (Cohen, Arkhipov, Braun, & Schulten, 2006) of VMD (Humphrey, Dalke, & Schulten, 1996). For each binding pose, the sulfonate group of Azo-NZ1 was considered a "particle" by replacing each of its atoms with a normalized Gaussian distribution (with width 1.5 times its atomic radius) and additively distributing those Gaussians on a three-dimensional grid (with dimensions $0.5 \times 0.5 \times 0.5$ Å^3). The resulting particle density is thus equivalent to the number of binding poses whose sulphonate group is located in a given volume of the pore.

The second approach was based on the analysis of the receptor–ligand interactions. First, the ligand binding poses were clustered using

the quality threshold algorithm implemented in VMD (https://github.com/luisico/clustering), and then the representative structure of the most populated cluster(s) was analysed using the Binana algorithm (Durrant & McCammon, 2011). The images of the modelling section were generated with UCSF Chimera (Pettersen et al., 2004) or VMD (Humphrey, Dalke, & Schulten, 1996).

2.8 | Nomenclature of targets and ligands

Key protein targets and ligands in this article are hyperlinked to corresponding entries in http://www.guidetopharmacology.org, the common portal for data from the IUPHAR/BPS Guide to PHARMACOLOGY (Harding et al., 2018), and are permanently archived in the Concise Guide to PHARMACOLOGY 2017/18 (Alexander et al., 2017).

3 | RESULTS

3.1 | Design of Azo-NZ1

The design of our photochromic ligand was based on the diazepam structure (Figure 1a), a widely used modulator of GABAergic function. Benzodiazepines are capable of binding in several interaction sites in the receptor (Middendorp, Maldifassi, Baur, & Sigel, 2015; Sieghart, 2015), and this offers, in principle, greater flexibility to introduce

relatively bulky substitutions like azobenzene without leading to a loss of functional activity of the compound. This choice was strengthened by the fact that the benzodiazepine nitrazepam, a diazepam derivative (Figure 1a), can be easily functionalized for a subsequent Mills reaction via reduction of its nitro-group (Severino et al., 2008) and thus be directly incorporated as part of the azobenzene (Figure 1b).

Therefore, the nitro-group of nitrazepam was reduced providing an aniline, which was used for further functionalization to set up the azo-bridge in a Mills-type reaction (see Section 2). To increase the solubility of the azo-nitrazepam, sulfanilic acid was used as precursor for the formation of the nitroso compound (Priewisch & Rück-Braun, 2005) providing a negative charge at physiological pH values (Kim, Gao, & Burgess, 2009). This compound showed robust photochromism with a preference for the *trans*-configuration in darkness and under visible light (455 nm), while under UV illumination (365 nm), the *cis*-configuration is favoured (Figures 1c,d and S11).

3.2 | Action of Azo-NZ1 on heteromeric GABA$_A$ α1/β2/γ2 receptors

Analysis of the GABA dose/response curves showed that EC$_{50}$ for α1/β2/γ2 GABA$_A$ receptors was 8 ± 3 μM (Figure 2a; n = 6), which was close to the previously reported values (Fisher, 2004). Diazepam (10 μM) co-applied with non-saturating concentration of GABA

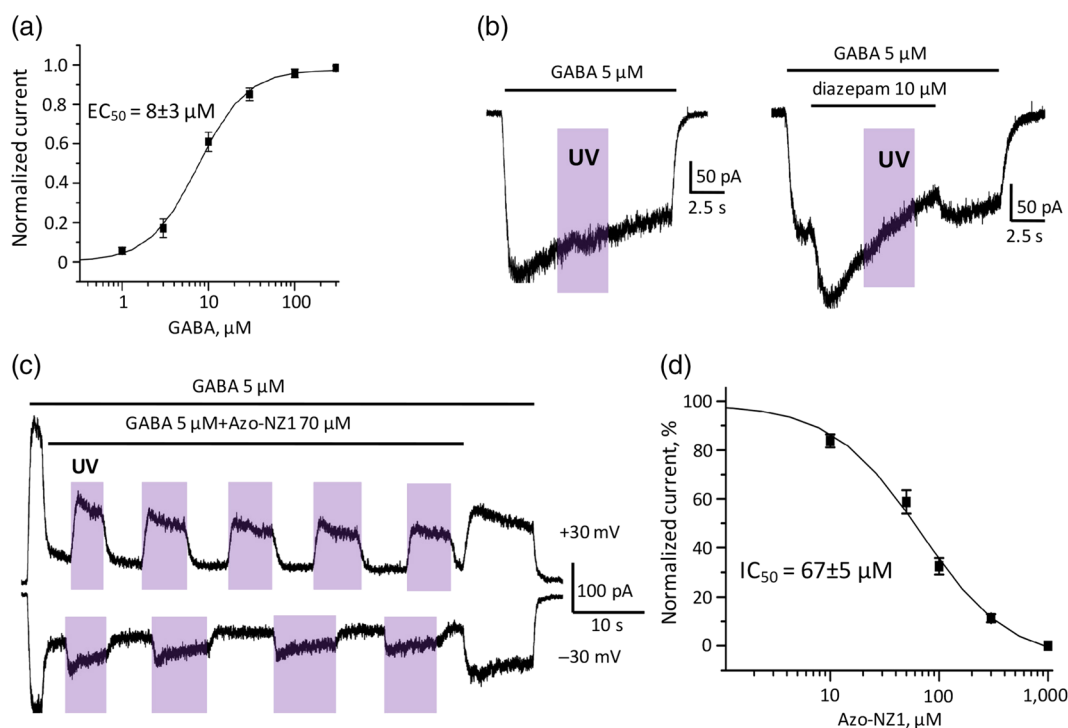**FIGURE 2**   Azo-NZ1 modulates activity of GABA$_A$ α1/β2/γ2 receptors in a UV-dependent manner. (a) Cumulative dose/response curve for GABA-induced currents in control conditions (n = 6). (b) Traces of currents induced by 5-μM GABA (left panel) and by co-application of 5-μM GABA with 10-μM diazepam (right panel) at V$_h$ = −30 mV. Durations of GABA and GABA/diazepam applications are indicated by black bars above the traces. Duration of UV illumination is indicated by violet rectangles. Note the absence of the effect of UV illumination on the responses. (c) Effect of 70-μM Azo-NZ1 on the amplitude of currents induced by 5-μM GABA at V$_h$ = +30 mV (top trace) and −30 mV (bottom trace). Note the stronger inhibition of currents by Azo-NZ1 at positive potentials. (d) Cumulative dose-response curve for Azo-NZ1 at GABA$_A$ receptors (n = 6)

caused an increase in the current amplitude (Figure 2b), which is in accordance with previous observations (Bormann & Clapham, 1985). UV illumination neither modified the currents induced by GABA nor by GABA plus diazepam (Figure 2b).

Ionic currents were evoked by 5 μM of GABA alone or with addition of Azo-NZ1. The photochromic compound in concentrations 0.5–1 μM did not produce effect on the GABA-induced currents, while application of Azo-NZ1 at 10 μM and higher concentrations caused its decreasing. As illustrated in Figure 2c, Azo-NZ1 at 70 μM produced a prominent decrease of the amplitude of $GABA_A$-mediated currents under visible light, when the compound was in *trans*-configuration. Illumination with UV light (365 nm) resulted in recovery of currents till values were close to the control. The degree of Azo-NZ1-induced suppression at positive potential was more pronounced: the amplitude of GABA-induced currents decreased by 78% and 51% at +30 mV and −30 mV, respectively (Figure 2c). Analysis of

concentration dependencies of Azo-NZ1 action shows that at −30 mV, the IC_{50} was 67 ± 5 μM ($n = 6$; Figure 2d), and thus, further experiments were performed with concentrations of Azo-NZ1 close to IC_{50}.

Using a "ramp" protocol (Figure 3c, inset), we have shown that, under visible light, 50-μM Azo-NZ1 decreased currents induced by 5-μM GABA by 76 ± 5% and 40 ± 4% at +60 mV and −60 mV, respectively ($n = 5$, $P < .05$), confirming that Azo-NZ1 is more efficient at positive potentials (Figure 3c). The recovery during UV illumination was not complete ($P < .05$), presumably, because of incomplete photoswitching of Azo-NZ1 in *cis*-configuration.

The voltage dependence of the inhibitory action of Azo-NZ1 suggested that the compound might act as an open channel blocker of $GABA_A$ receptors (Maleeva, Peiretti, Zhorov, & Bregestovski, 2017). To test this hypothesis, we compared the action of Azo-NZ1 at different concentrations of the agonist. The amplitude of currents induced
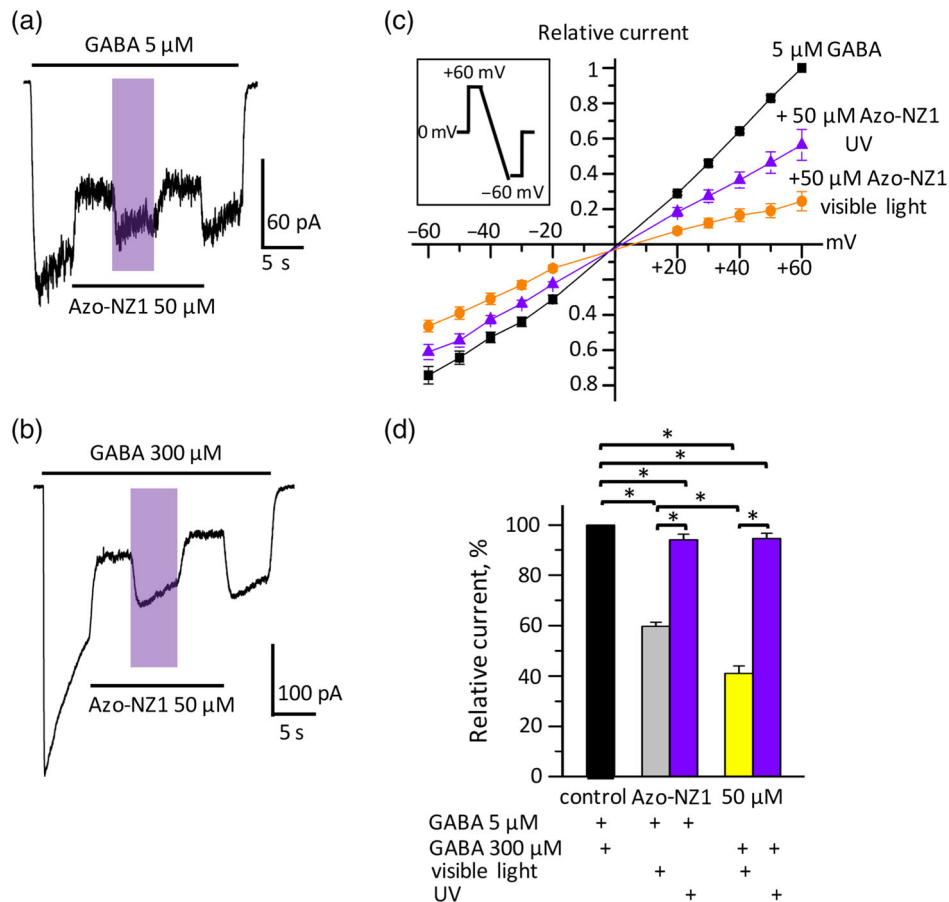

FIGURE 3 Strength of suppression of $GABA_A$ receptors by Azo-NZ1 depends on the membrane potential and becomes stronger at higher agonist concentration. (a) Representative trace of the current induced by application of 5-μM GABA and by co-application of 5-μM GABA with 50-μM Azo-NZ1, V_{hold} = −30 mV. (b) Representative recording of the current induced by saturating concentration of GABA (300 μM) and by a mixture of 300-μM GABA with 50-μM Azo-NZ1, V_{hold} = −30 mV. (c) Cumulative current-voltage relationship curves obtained during application of 5-μM GABA, a mixture of 5-μM GABA with 50-μM Azo-NZ1 at visible light, and GABA + Azo-NZ1 upon UV illumination ($n = 5$). Scheme of the ramp protocol is presented in the inset on the left. (d) Summary of $GABA_A$ receptor-mediated suppression induced by Azo-NZ1. Mean relative amplitude (%) of currents induced by a mixture of Azo-NZ1 with low (5 μM) and saturating (300 μM) concentrations of GABA at visible light and upon UV illumination. Grey column: 5-μM GABA +50-μM Azo-NZ1 at visible light; yellow column: 300-μM GABA +50-μM Azo-NZ1 at visible light; violet columns: 5- or 300-μM GABA +50-μM Azo-NZ1 at UV illumination. Data are presented as mean ± SEM; V_{hold} = −30 mV summary from six to eight cells, $*P < .05$

by GABA concentration below EC_{50} (5 μM) was decreased by application of Azo-NZ1 (50 μM) (Figure 3a,d). Azo-NZ1 co-applied with saturating concentration of GABA (300 μM) produced an even stronger inhibitory effect (Figure 3b,d). Thus, Azo-NZ1 acts as a non-competitive antagonist of $GABA_A$ receptors, and its binding does not coincide with the agonist-binding site. In both cases, UV illumination restores current amplitude, though not completely, close to the control values.

3.3 | Action of Azo-NZ1 on homomeric ρ1 and ρ2 $GABA_A$ ($GABA_C$) receptors

To further investigate the hypothesis that Azo-NZ1 acts as a blocker of the GABA receptor channels without interacting with the diazepam-binding site located at the α/γ subunits interface, we analysed the action of this photochromic ligand on benzodiazepine-insensitive ρ1 and ρ2 $GABA_A$ ($GABA_C$) homomeric receptors. Concentration-dependency analyses showed that the EC_{50} for GABA of ρ1 and ρ2 $GABA_C$ receptors were similar (Figure 4a). In accordance with previous observations (Ragozzino et al., 1996), GABA-induced currents

mediated by these receptors do not exhibit desensitization and are characterized by a very long deactivation period after agonist application.

We found that Azo-NZ1 did not alter the activity of human ρ1 $GABA_C$ receptors (Figure 4b), but it enabled robust photoswitching of ρ2 receptors (Figure 4d). The IC_{50} for GABA ρ2 receptors comprised 128 ± 25 μM (n = 6), and thus, all the experiments with ρ2 receptors were performed at 100 μM of Azo-NZ1, as this concentration was close to IC_{50} (Figure 4f). Under visible light, currents induced by saturating GABA concentration (10 μM) were decreased by 100-μM Azo-NZ1 at −30 and +30 mV, respectively (Figure 4d,e), that is, the inhibitory action of Azo-NZ1 on ρ2 receptors is also voltage-dependent. UV illumination restored the amplitude of the current to the nearly control values. The amplitude of ρ2 currents induced by 10 μM of GABA without addition of Azo-NZ1 was not affected by UV illumination (Figure 4c).

3.4 | Molecular determinants of Azo-NZ1 action

The well-defined voltage dependence of the Azo-NZ1 effect on $GABA_A$ and $GABA_C$ ρ2 receptors and its independence on the
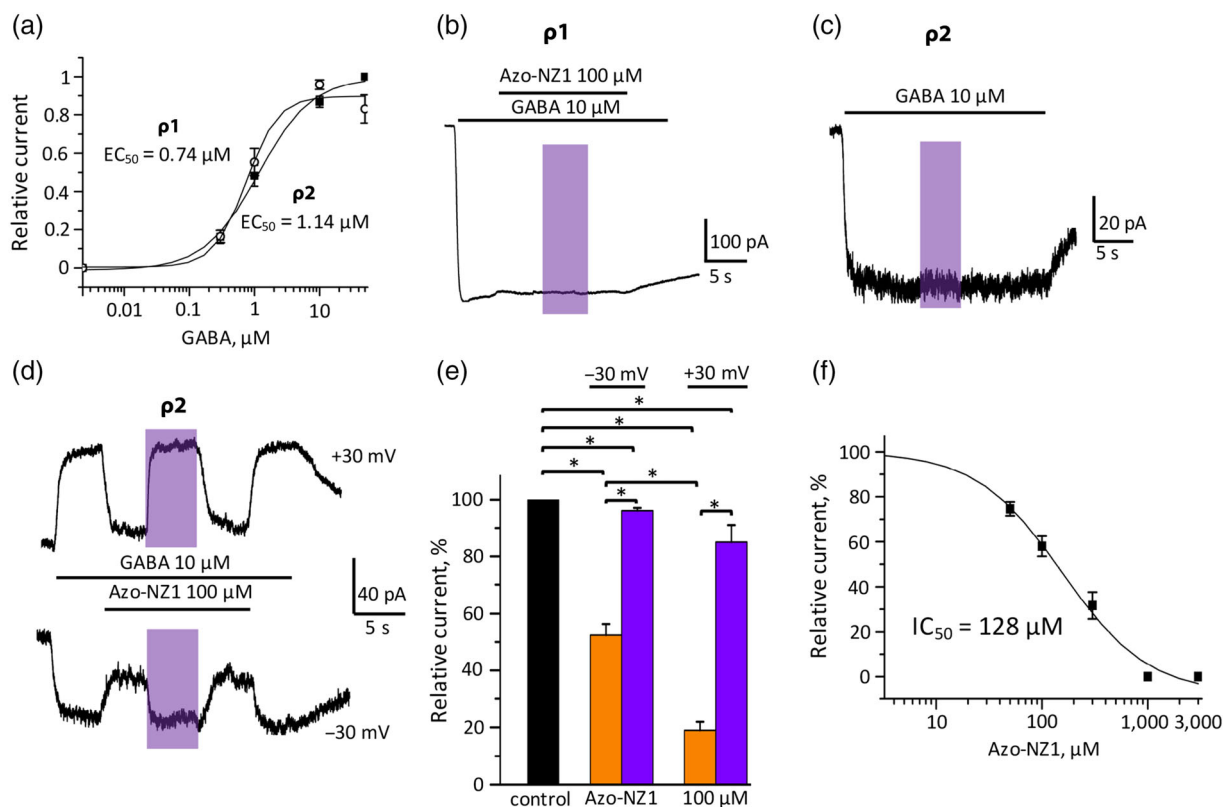

FIGURE 4 Azo-NZ1 decreases currents via $GABA_{Cρ}$ ρ2 receptors in a UV-dependent manner, while being not active at $GABA_C$ ρ1 receptors. (a) Cumulative dose-response curves for GABA at $GABA_C$ ρ1 and $GABA_C$ ρ2 receptors. (b) Representative trace illustrating the absence of Azo-NZ1 effect on $GABA_C$ ρ1 receptors at visible and UV light. (c) Representative trace of GABA ρ2-mediated current induced by application of GABA 10 μM at visible light and upon UV illumination. Note the absence of UV effect on the amplitude of GABA-induced current. (d) Representative traces of $GABA_C$ ρ2 currents induced by 10-μM GABA and by a mixture of 10-μM GABA with 100-μM Azo-NZ1 at +30 mV (upper panel) and at −30 mV (lower panel). (e) The relative amplitudes of $GABA_C$ ρ2-mediated currents suppressed by Azo-NZ1 (100 μM): at +30 and −30 mV in control (GABA 10 μM), after application of Azo-NZ1 in visible light (orange column) and upon UV illumination (violet column). Mean ± SEM, n = 6–10, *P < .05. (f) Cumulative dose-response curve for Azo-NZ1 at GABA ρ2 receptors (n = 6)
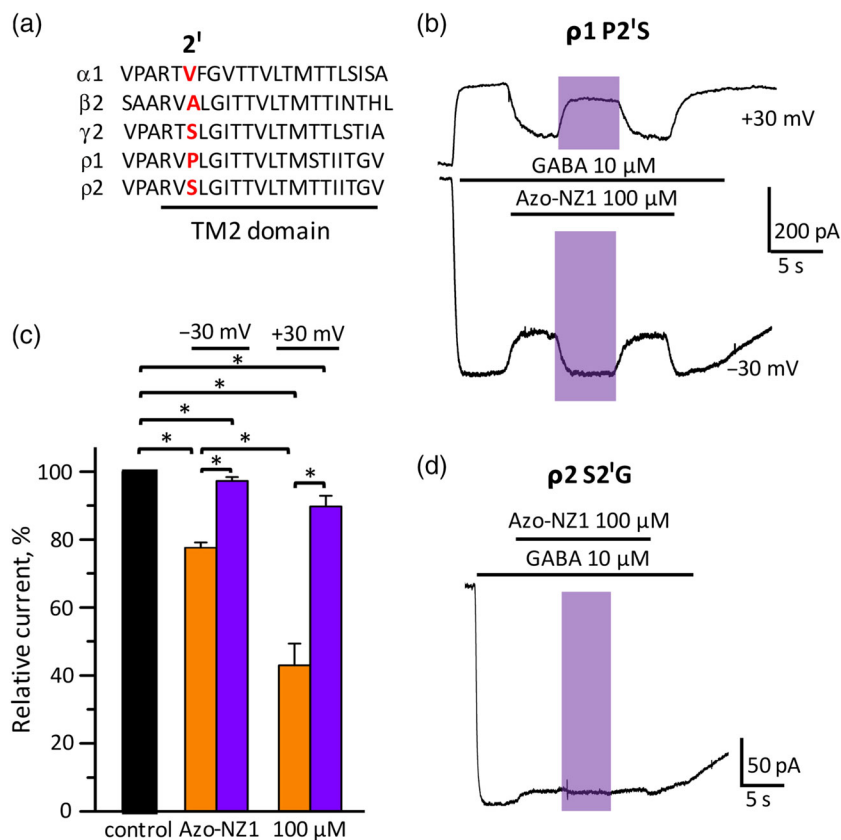
FIGURE 5 Effect of Azo-NZ1 on mutant ρ1 and ρ2 GABA$_C$ receptors. (a) Amino acid sequence alignment of GABA receptors subunits TM2 Cl-selective pore. Amino acids in 2′ position are highlighted in red. Note the high identity of the TM2 sequences between ρ1 and ρ2 subunits. (b) Representative traces of currents mediated by GABA ρ1 P2′S receptors suppressed by 100-μM Azo-NZ1 application at −30 and +30 mV. (c) Relative amplitude of GABA-induced currents mediated by ρ1 P2′S receptors at +30 and −30 mV in control (10-μM GABA), at application of 100-μM Azo-NZ1 in visible light (orange column) and upon UV illumination (violet column). Mean ± SEM, n = 7, *P < .05. (d) Representative trace depicting the absence of Azo-NZ1 effect at ρ2 mutant S2′G receptors

agonist concentration strongly suggest that Azo-NZ1 in *trans*-configuration blocks the ion pore of these receptors. It is well documented that the position 2′ of the pore-forming transmembrane domain 2 (TM2) is crucial for the action of several pore-blocking molecules in Cys-loop receptors, including GABA$_C$ receptors (Xie, Song, Ripps, & Qian, 2008). An amino acid sequence alignment showed that TM2 domains of ρ1 and ρ2 subunits differ by the amino acids at the position 2′: ρ1 contains proline while ρ2 contains a serine residue (Figure 5a).

To check the putative role of the 2′ residue in Azo-NZ1 sensitivity, we substituted proline by serine at position 2′ of the ρ1 subunit. P2′S mutation did not affect the apparent affinity of the ρ1 receptor to GABA (EC$_{50}$ = 0.98, n = 4) but made it sensitive to the action of Azo-NZ1. Under visible light, 100-μM Azo-NZ1 inhibited currents induced by saturating concentrations of 10-μM GABA (Figure 5b,c). UV illumination caused recovery of currents to 97 ± 1% and 90 ± 3%, respectively (Figure 5b).

Thus, we confirmed that Azo-NZ1 in its *trans*-configuration interacts with the pore of GABA receptors and identified the 2′ position of the TM2 domain as key determinant of the light-dependent action of Azo-NZ1. This conclusion was additionally confirmed in experiments demonstrating that the S2′G mutation in the ρ2 subunit influenced its interaction with Azo-NZ1. Upon application of Azo-NZ1 currents amplitude decreased by 14 ± 2% (Figure 5d, n = 5, P < .05), which might be due to weak interaction between Azo-NZ1 and mutant receptor; importantly, UV effect was virtually absent. Results

of the modelling analysis presented below are in line with our observations.

3.5 | Interaction of Azo-NZ1 with other members of Cys-loop receptor family

GABA receptors and glycine receptors belong to the Cys-loop receptors family and amino acid sequences forming their Cl-selective pores are highly similar (Figure S1A). Thus, we asked if Azo-NZ1 also acted as a glycine receptor channel blocker.

Trans-Azo-NZ1 produced only minor inhibitory effect in α1 glycine receptors—the current amplitude was reduced to 86 ± 3% (Figure S1B, n = 4, P < .05), with slightly stronger reduction upon illumination with UV light (to 73 ± 2%, P < .05). In contrast, in α2 glycine receptors, Azo-NZ1 induced a prominent decrease of the current amplitude (to 23 ± 3%, n = 10, P < .01) that was altered by UV illumination (95 ± 7%, P < .01, n = 10; Figure S1B,C). The profile of α2 glycine receptor interaction with Azo-NZ1 strongly resembles the one of GABA$_A$ and GABA$_C$ receptors, suggesting the same pore-blocking mechanism of action.

In order to have a wider view of Azo-NZ1 selectivity profile, we also tested it in a cation-selective member of Cys-loop receptor family, the 5HT$_3$A receptor. In contrast to GABA receptors and glycine receptors, Azo-NZ1 in *trans* or *cis*-configurations did not interact in a specific manner with 5-HT3A receptors (Figure S2, Supplementary

Text). Thus, Azo-NZ1 selectively interacts with anion-permeable channels of the Cys-loop receptor family, exhibiting a subunit specificity based on the nature of 2′ residues in TM2 pore.

3.6 | Modelling of Azo-NZ1 molecular interactions with GABA receptors

To get further insights into the mechanism of action of Azo-NZ1 in GABA receptors, we performed molecular docking calculations. In view of the mutagenesis results indicating the relevance of the 2′ residues, the docking was carried out in the transmembrane region of the ion channel pore. Four different GABA$_C$ receptor structures were used: wild-type ρ2, S2′G ρ2 mutant, wild-type ρ1, and P2′S ρ1 mutant (see Section 2); all structures were modelled in the open channel state.

Docking of *trans*-Azo-NZ1 to the GABA$_C$ ρ2 receptor (Figure 6a) showed that the preferred binding site of the sulfonate group is located in the narrow 2′ position of the pore region (Figure S3A), at the centre of the ring formed by five serine residues (Figure 6b). Such a ligand orientation creates a strong hydrogen bond network involving the sulfonate oxygen atoms and the hydroxyl groups. In addition, a hydrogen bond between the hydroxyl group of one of the T13′ residues and the carbonyl of the nitrazepam core of Azo-NZ1 holds the ligand in a linear orientation almost parallel to the pore axis. Further stabilization is provided by hydrophobic interactions involving the apolar region of the nitrazepam core, the side chain of L9′ and the methyl group of T6′ (Figure 6b). The length of the ligand (14 Å) is optimal to place its polar groups (sulfonate and amido) close to the polar side chains of S2′ and T13′, respectively, which are separated by 16 Å. In addition, the size of the sulfonate group is comparable with
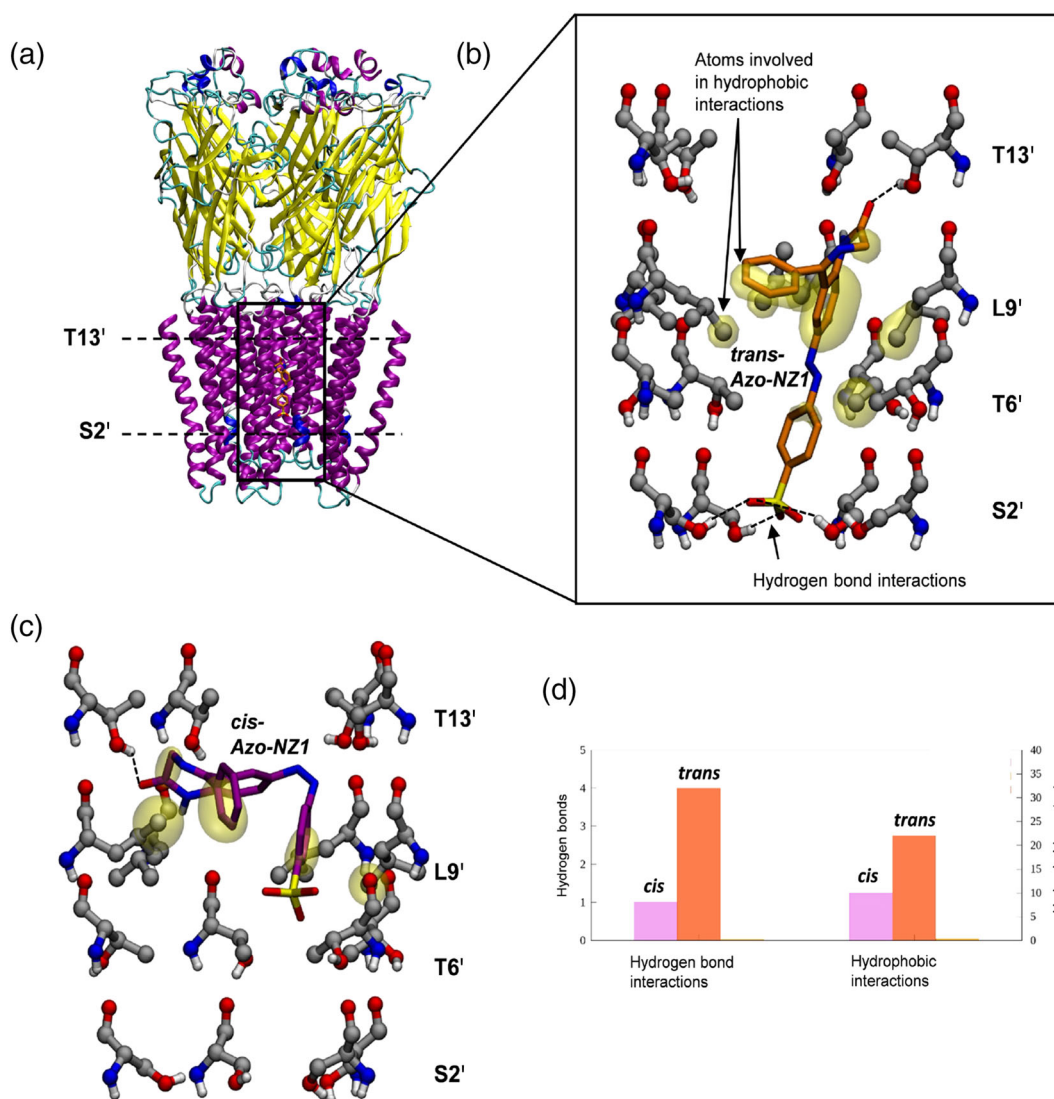

FIGURE 6 Results of the docking of Azo-NZ1 in the transmembrane part domain of ρ2 GABA$_C$ receptor. (a) Tridimensional view of the ρ2 GABA$_C$ receptor. The S2′ and T13′ positions are marked with dashed lines. (b) Most likely docking pose of the *trans*-isomer in the transmembrane domain. The interior of the pore is shown as viewed from the intracellular part. (c) Most likely pose for the *cis*-isomer in the transmembrane domain. The interior of the pore is shown as viewed from the extracellular part. (d) Relative number of intermolecular interactions formed by the *cis*- and *trans*-isomers of Azo-NZ1 with residues of the transmembrane domain of ρ2 GABA$_C$ receptor

the pore diameter at the level of the 2′ serine ring, thus creating an obstacle that hinders the passage of the chloride ions through the pore both sterically and electrostatically (Figure S4). Interestingly, the negatively charged sulfonate group occupies the same position as the chloride ion trapped in X-ray structures of $GABA_A$ receptor (Laverty et al., 2017) and glycine receptor (Du, Lü, Wu, Cheng, & Gouaux, 2015). Altogether, the architecture of *trans*-Azo-NZ1 fits perfectly in the pore region of the $GABA_C$ ρ2 receptor.

In contrast, the position of the sulfonate group of *cis*-Azo-NZ1 is more scattered all over the 2′-13′ region of the pore (Figure S3B), and the number of poses with the sulfonate group in the 2′ region (i.e., the ones able to block the pore) is decreased by half. Analysis of the preferred binding pose of the ligand (Figure 6c) shows that, due to the staple-like shape of *cis*-Azo-NZ1, the ligand is preferentially located further up in the pore and the number of interactions with the receptor is dramatically decreased compared to the *trans*-isomer (Figure 6d). The ligand forms only one hydrogen bond with the pore residues, involving the tertiary amine of the benzodiazepine core and one hydroxyl group of T13′, and most importantly, the sulfonate group does not form any interaction with the pore-lining residues, since it is positioned near L9′. The smaller number of interactions of the *cis*-isomer compared to *trans* indicates that the ligand will have a

higher probability of dissociation upon UV irradiation. Moreover, the ligand is mostly placed in the regions where the diameter of the pore is wider (around 11 Å, see Figure S4), and thus, it cannot block chloride conduction by either steric or electrostatic effects. Therefore, we predict that, even if *cis*-Azo-NZ1 remains bound, it would not decrease the channel current of the receptor. These results explain the higher capability of *trans*-Azo-NZ1 to block the pore of the $GABA_C$ ρ2 receptor compared to the *cis*-isomer.

The importance of 2′ residues is also corroborated by the results obtained for the S2′G ρ2 mutant. In this case, the sulfonate group cannot form hydrogen bonds with the 2′ residues. As a consequence, the population of *trans*-Azo-NZ1 in the 2′ region decreases and the ligand is no longer able to block the pore (Figures S5B and S6A). Similar results were also obtained for the ρ1 receptor, which has proline at the 2′ region (Figures S6B and S7A). Conversely, mutation of proline to serine (P2′S) in the ρ1 receptor increases the population of the sulfonate in the 2′ region (Figure S7B) with respect to the WT receptor (Figure S7A). The associated binding mode of Azo-NZ1 to P2′S ρ1 (Figure S6C) is very similar to the one for wild-type ρ2 (Figure 6), consistent with the appearance of inhibition observed in our experiments (Figure 5).

We also performed docking calculations for the heteromeric α1/β2/γ2 $GABA_A$ receptor, using a model of the open channel state
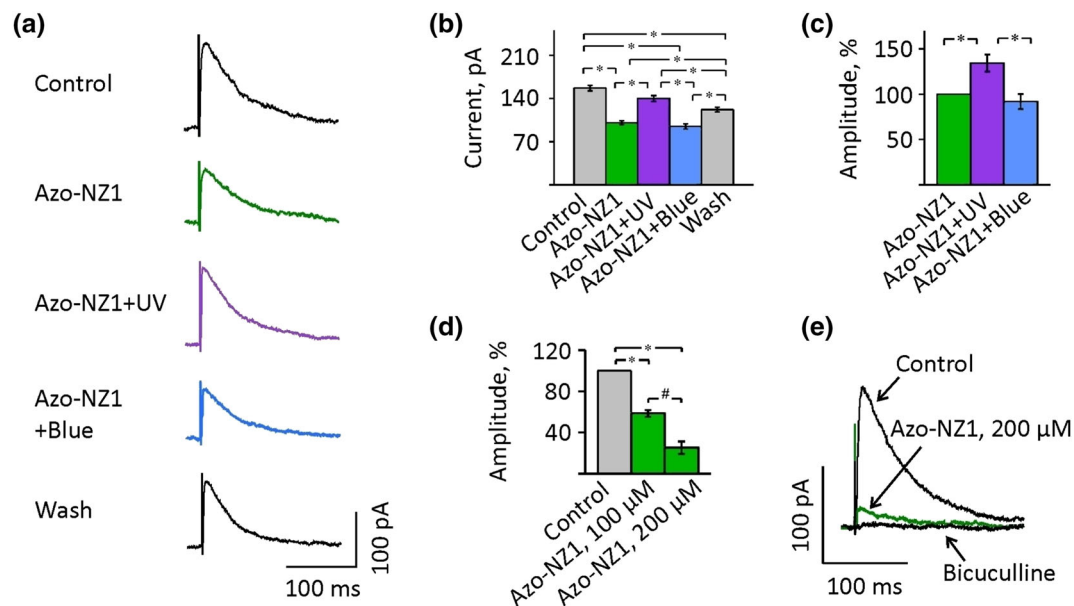

FIGURE 7 Effect of Azo-NZ1 on the GABAergic postsynaptic currents in brain slices. (a) Traces of average evoked GABAergic postsynaptic currents (eIPSCs) recorded from dentate gyrus granule cells in the adult mice hippocampal slices: in the control conditions (Control); after addition to aCSF of 100-μM Azo-NZ1 (Azo-NZ1); during perfusion of the slice with UV-illuminated aCSF +100-μM Azo-NZ1 (Azo-NZ1 + UV); during perfusion with blue light-illuminated aCSF +100-μM Azo-NZ1 (Azo-NZ1 + blue); 2–3 min of washing by aCSF (Wash). Each trace represents average of seven to 10 individual eIPSCs induced by stimulation with theta-tube electrode placed in the granule cell layer. V_h = 0 mV. (b) Summary of the mean amplitudes of GABAergic eIPSCs recorded in control conditions; in the presence of 100-μM Azo-NZ1, at illumination either at 365 nm (purple column) or 455 nm (green column). Data from the experiment presented in (a). Whiskers area reflects the standard error range. *Significant difference with $P < .05$ (two-sample *t* test, n = 7–10). (c) Mean percentages of the eIPSCs amplitude potentiation in the presence of 100-μM Azo-NZ1 by UV illumination. *Significant difference with $P < .05$ (paired sample Wilcoxon signed rank test, n = 5). (d) Summary of the percentages of the eIPSC amplitude decrease in the presence of 100- and 200-μM Azo-NZ1 at blue light illumination. */#Significant difference with $P < .05$ (paired sample Wilcoxon signed rank test and Mann–Whitney *U* test, respectively; n = 5). (e) Superimposed traces of eIPSCs illustrating decrease of currents at addition of 200-μM Azo-NZ1 and 10-μM bicuculline. Note the complete suppression of events by bicuculline. Each trace represents average of six to 10 individual eIPSCs. V_h = 0 mV

(Bergmann, Kongsbak, Sørensen, Sander, & Balle, 2013). For this receptor, the density analysis results are noisier due to the heterogeneous subunit composition (Figure S8A). Therefore, we can only say with certainty that the *trans*-Azo-NZ1 binding mode with the sulphonate bound at position 2′ is the most likely, similar to homomeric ρ2 GABA$_C$ receptor. Even though there is only one serine in this region (belonging to the γ2 subunit), the hydrogen bond interaction with the ligand is still present (Figure S8B). Moreover, although α1-Val2′ and β2-Ala2′ are not able to form hydrogen bonds, their volume is similar to that of Ser and thus still compatible with sulphonate binding at position 2′. In addition, the hydrogen bond between the carbonyl group of Azo-NZ1 and T13′ is also maintained (Figure S8B). As a result, *trans*-Azo-NZ1 is clamped in the pore of the GABA$_A$ receptor (Figure S8C), as it was in the GABA$_C$ ρ2 receptor (Figure 6b) and thus is able to block chloride conduction.

Altogether, these observations demonstrate that Azo-NZ1 is a photoswitchable blocker of GABA$_A$ and GABA$_C$ receptors, whose *trans*-configuration interacts with residues located in the pore, in particular at positions 2′ and 13′. In *trans*-Azo-NZ1, the distance between the sulphonate group and the carbonyl group of the benzodiazepine core is optimal for Azo-NZ1 to get clamped between these two residues, enabling pore blocking.

3.7 | Effect of Azo-NZ1 on synaptic currents in brain slices

Finally, to evaluate Azo-NZ1 as photochromic modulator of GABAergic synaptic events, we performed electrophysiological recordings from neurons in dentate gyrus granular layer, which possess a strong GABAergic synaptic inputs (Coulter & Carlson, 2007; Haselmann, Röpke, Werner, Kunze, & Geis, 2015).

Whole-cell recordings were performed at V_h = 0 mV and stimulation pulses induced by theta pipettes delivered at frequency 0.1 Hz, inducing a reliable GABAergic eIPSCs, which exhibited relatively low run-down (about 20%) during long-lasting recordings (>1 hr). In control conditions, amplitudes of eIPSCs varied in different neurons between 50 and 400 pA (*n* = 10).

For the neuron illustrated in the Figure 7a,b, amplitude of eIPSCs in control aCSF was 156.9 ± 4.5 pA, and it decreased to 100.6 ± 3.2 pA after addition of 100-μM Azo-NZ1. Switching to the solution preilluminated with UV light (365 nm) caused an elevation of the amplitude, while the successive illumination with 455 nm resulted in its decrease. After washing with pure aCSF, the amplitude of eIPSCs recovered to near control value. Similar degrees of the light-induced modulation was observed on five other neurons (Figure 7c). Application of 200-μM Azo-NZ1 caused much more pronounced inhibition (Figure 7d,e). On average, the suppression of eIPSCs amplitude by 100 and 200 μM of Azo-NZ1 was to 58.6 ± 3.3% and 25.2 ± 6.0%, respectively (Figure 7d). Bicuculline at 10 μM caused complete inhibition of eIPSCs ensuring the GABAergic nature of the events (Figure 7e).

These observations demonstrate that Azo-NZ1 causes suppression of synaptic GABAergic currents in a light-dependent manner.

4 | DISCUSSION

Our study presents an azobenzene-nitrazepam-based photochromic compound (Azo-NZ1) and characterization of its action on Cys-loop receptors. Using electrophysiological, mutational, and molecular modelling analysis, we demonstrate that Azo-NZ1 is a light-controllable channel blocker of heteromeric GABA$_A$, homomeric GABA$_C$ ρ2 receptors and α2 glycine receptors, heterologously expressed in cultured cells, as well as modulator of synaptic GABAergic currents in dentate gyrus neurons of hippocampal brain slices. Our attention was mostly focused on the action of Azo-NZ1 at GABA receptors as they are the predominant subtype of inhibitory ligand-gated receptors in higher brain regions (Bowery et al., 1984; Sieghart & Sperk, 2002).

4.1 | Azo-NZ1 as Cl-channel blocker

Surprisingly, in our experiments, Azo-NZ1 caused an inhibitory effect on the GABA$_A$ receptor, contrary to the potentiating effects via benzodiazepines binding sites. Moreover, similar inhibition was observed for GABA ρ2, which lacks the classical benzodiazepine site (Sieghart, 2015), and for α2 glycine receptors. While we cannot entirely rule out the allosteric interaction of Azo-NZ1, the absence of modulation at nM concentrations and docking calculations (see Supporting Information) suggest that the functional effects of Azo-NZ1 via the classical benzodiazepine site are negligible.

Our results strongly suggest that the photochrome acts as a blocker of GABA receptors Cl-selective pore, interacting primarily with the 2′ position of the TM2 domain of the channel. The following results support the role of Azo-NZ1 as GABA receptor pore blocker:

i. Azo-NZ1-induced suppression becomes stronger upon elevation of GABA concentrations;

ii. the effect of Azo-NZ1 is voltage dependent, being much stronger at positive membrane potentials;

iii. mutation in the ρ1 GABA$_C$ receptor of a single amino acid situated at the 2′ level of the ion pore (P2′S) resulted in the appearance of blocking activity of Azo-NZ1, with features similar to GABA$_C$ ρ2 receptors;

iv. the S2′G mutation in ρ2 subunits resulted in the loss of the Azo-NZ1 specific activity;

v. molecular docking calculations show that the length of *trans*-Azo-NZ1 fits in the pore region, with the sulfonate group blocking ion passage at the 2′ region.

In our experiments, we have achieved a robust photoswitching effect using Azo-NZ1. Upon UV irradiation, currents recovered to 85–97%. The remaining 15–3% might be explained by not complete switching of *trans*-Azo-NZ1 into *cis*-state, not complete dissociation of *cis*-Azo-NZ1 form the pore, or fast development of the receptor desensitization.

4.2 | Possible mechanism of Azo-NZ1 interaction with the channel

The 2′ residue of the TM2 domain (see Figure 5a) is a key region that determines the action of several pore blockers of Cys-loop receptors, including cyanotriphenylborate (Rundström et al., 1994), picrotoxin (Lynch, Rajendra, Barry, & Schofield, 1995; Zhorov & Bregestovski, 2000), niflumic acid (Maleeva, Peiretti, Zhorov, & Bregestovski, 2017), and cyclothiazide (Xie, Song, Ripps, & Qian, 2008). The Azo-NZ1 construct contains two features that are essential to impart sensitivity to the photochrome: (a) the negative charge of the sulphonate group (mimicking that of the chloride ion) and (b) the distance between this sulphonate group and the carbonyl group of the benzodiazepine core (see Figure S2). In *trans*-Azo-NZ1, this distance is optimal (~14.1 Å) to bridge the two pore-lining hydrogen bond residues S2′ and T13′. Upon UV light irradiation, *cis*-Azo-NZ1 may either remain in the channel (assuming another binding conformation that unblocks the pore) or exit the channel (reaching the bath solution). Although with the data at hand we cannot distinguish between the two possibilities, it is feasible that *cis*-Azo-NZ1 remains partially bound in the pore, as can be suggested from Figures 3c and 7b and modelling analysis (Figure 6c).

4.3 | Effect of Azo-NZ1 on synaptic currents

Our analysis on dentate gyrus neurons from mouse brain slices demonstrated that Azo-NZ1 decreases amplitude of GABAergic synaptic events in a light-dependent manner. The inhibition was weaker in comparison with the one observed at heterologously expressed α1/β2/γ2 GABA$_A$ receptors. This may result from the different composition of GABA receptors receptors present in the dentate gyrus neurons, which can express up to 10 GABA$_A$ receptor subunits, as single-cell mRNA analysis demonstrated (Brooks-Kayal, Shumate, Jin, Rikhter, & Coulter, 1998; Coulter & Carlson, 2007). Also, synaptic and extrasynaptic GABA$_A$ receptors with distinctive properties and subunit composition can be differently modulated by the photochrome. The role of these discrepancies in the neuronal circuit modulation by Azo-NZ1 should be clarified in future studies.

Recently, several photochromic modulators of GABA$_A$ receptors were developed (reviewed in Bregestovski, Maleeva, & Gorostiza, 2018): two potentiators (Stein et al., 2012; Yue et al., 2012) and several inhibitors (Huckvale, Mortensen, Pryde, Smart, & Baker, 2016; Lin et al., 2014, 2015; Lin, Tsai, Rajappa, & Kramer, 2018). The compounds developed by Lin et al. are required to be tethered to the receptor, which needs specific mutation of the GABA receptor, that is, genetic manipulation. The compound developed by Huckvale et al. is a soluble photochromic competitive GABA receptor antagonist based on combination of azobenzene and gabazine. Azo-NZ1, presented in our study, exhibits a completely different mode of action, being a light-controlled blocker of ionotropic GABA receptor channels. Moreover, Azo-NZ1 is the first known photochromic modulator of ρ2 GABA$_C$ receptors that are highly expressed in retina. Azo-NZ1 blocks

as well α2 glycine receptors in a similar UV-dependent manner, probably due to highly conserved amino acid sequences of pore-forming domains of GABA and glycine receptors. Indeed, the difference in Azo-NZ1 action on α1 and α2 glycine receptors, caused by glycine to alanine substitution in 2′ position of their TM2 domains, confirms the pore-blocking effect of Azo-NZ1. In contrast, Azo-NZ1 was not able to block the 5-HT$_3$A receptor, a cation-selective member of Cys-loop receptor superfamily.

Our findings pave the way for development of a novel pharmacological toolset for photo-modulation, as well as functional and molecular physiology studies of these receptors. Azo-NZ1 is a freely diffusible ligand that binds to endogenous receptors, and such studies could be carried out without any genetic manipulations. Photocontrol of inhibitory neurotransmission should be readily accessible in acute preparations and in all kinds of vertebrate and invertebrate wild-type animals using Azo-NZ1.

CONFLICT OF INTEREST

The authors declare no conflicts of interest.

AUTHOR CONTRIBUTIONS

G.M., E.P., and A.G.-J. performed the experiments. A.B.-B., D.W. and K.R. synthesized the compounds. A.N.-H. and M.A.-P. performed the molecular modelling. F.P. and P.S. performed the mutagenesis. G.M., K.R., A.N.-H., M.A.-P., C.R., B.K., P.G., P.B. analysed the data and wrote the manuscript. M.A.-P., C.R., B.K., P.G., P.B. supervised the project, reviewed, discussed, and conceptualized data.

DECLARATION OF TRANSPARENCY AND SCIENTIFIC RIGOUR

This Declaration acknowledges that this paper adheres to the principles for transparent reporting and scientific rigour of preclinical research as stated in the *BJP* guidelines for Design & Analysis, and Animal Experimentation, and as recommended by funding agencies, publishers and other organisations engaged with supporting research.

ORCID

Karin Rustler https://orcid.org/0000-0001-6548-1333
Mercedes Alfonso-Prieto https://orcid.org/0000-0003-4509-4517
Pau Gorostiza https://orcid.org/0000-0002-7268-5577
Piotr Bregestovski https://orcid.org/0000-0003-2699-7825

REFERENCES

Alexander, S. P. H., Peters, J. A., Kelly, E., Marrion, N., Benson, H. E., Faccenda, E., ... Davies, J. A. (2015). The Concise Guide to PHARMACOLOGY 2015/16: Ligand-gated ion channels. *British Journal of Pharmacology*, *172*(24), 5870–5903. https://doi.org/10.1111/bph.13878

Alexander, S. P. H., Peters, J. A., Kelly, E., Marrion, N. V., Faccenda, E., Harding, S. D., ... CGTP Collaborators. (2017). The Concise Guide to PHARMACOLOGY 2017/18: Ligand-gated ion channels. *British Journal of Pharmacology*, *174*, 130–S159. https://doi.org/10.1111/bph.13879

Bergmann, R., Kongsbak, K., Sørensen, P. L., Sander, T., & Balle, T. (2013). A unified model of the GABA_A receptor comprising agonist and benzodiazepine binding sites. *PLoS ONE*, *8*(1), e52323. https://doi.org/10.1371/journal.pone.0052323

Biasini, M., Bienert, S., Waterhouse, A., Arnold, K., Studer, G., Schmidt, T., ... Schwede, T. (2014). SWISS-MODEL: Modelling protein tertiary and quaternary structure using evolutionary information. *Nucleic Acids Research*, *42*(W1), W252–W258. https://doi.org/10.1093/nar/gku340

Bormann, J., & Clapham, D. E. (1985). γ-Aminobutyric acid receptor channels in adrenal chromaffin cells: A patch-clamp study. *Proceedings of the National Academy of Sciences*, *82*(7), 2168–2172. https://doi.org/10.1073/pnas.82.7.2168

Bowery, N. G., Price, G. W., Hudson, A. L., Hill, D. R., Wilkin, G. P., & Turnbull, M. J. (1984). GABA receptor multiplicity: Visualization of different receptor types in the mammalian CNS. *Neuropharmacology*, *23*(2), 219–231. https://doi.org/10.1016/0028-3908(84)90063-7

Bregestovski, P., Maleeva, G., & Gorostiza, P. (2018). Light-induced regulation of ligand-gated channel activity. *British Journal of Pharmacology.*, *175*, 1892–1902. https://doi.org/10.1111/bph.14022

Brooks-Kayal, A. R., Shumate, M. D., Jin, H., Rikhter, T. Y., & Coulter, D. A. (1998). Selective changes in single cell GABA_A receptor subunit expression and function in temporal lobe epilepsy. *Nature Medicine*, *4*(10), 1166–1172. https://doi.org/10.1038/2661

Cohen, J., Arkhipov, A., Braun, R., & Schulten, K. (2006). Imaging the migration pathways for O2, CO, NO, and Xe inside myoglobin. *Biophysical Journal*, *91*(5), 1844–1857. https://doi.org/10.1529/biophysj.106.085746

Coulter, D. A., & Carlson, G. C. (2007). Functional regulation of the dentate gyrus by GABA-mediated inhibition. *Progress in Brain Research*, *163*, 235–812.

Du, J., Lü, W., Wu, S., Cheng, Y., & Gouaux, E. (2015). Glycine receptor mechanism elucidated by electron cryo-microscopy. *Nature*, *526*(7572), 224–229. https://doi.org/10.1038/nature14853

Durrant, J. D., & McCammon, J. A. (2011). BINANA: A novel algorithm for ligand-binding characterization. *Journal of Molecular Graphics and Modelling*, *29*(6), 888–893. https://doi.org/10.1016/j.jmgm.2011.01.004

Fisher, J. L. (2004). A mutation in the GABA_A receptor α1 subunit linked to human epilepsy affects channel gating properties. *Neuropharmacology*, *46*(5), 629–637. https://doi.org/10.1016/j.neuropharm.2003.11.015

Frisch, M. J., Trucks, G. W., Schlegel, H. B., Scuseria, G. E., Robb, M. A., Cheeseman, J. R., ... Nakatsuji, H. (2013). *GAUSSIAN09. Revision D.01*. USA: Gaussian Inc., Wallingford, CT.

Gielen, M., Thomas, P., & Smart, T. G. (2015). The desensitization gate of inhibitory Cys-loop receptors. *Nature Communications*, *6*, 6829. https://doi.org/10.1038/ncomms7829

Gorostiza, P., & Isacoff, E. Y. (2008). Nanoengineering ion channels for optical control. *Physiology*, *23*(5), 238–247. https://doi.org/10.1152/physiol.00018.2008

Guandalini, L., Cellai, C., Laurenzana, A., Scapecchi, S., Paoletti, F., & Romanelli, M. N. (2008). Design, synthesis and preliminary biological evaluation of new hydroxamate histone deacetylase inhibitors as potential antileukemic agents. *Bioorganic & Medicinal Chemistry Letters*, *18*(18), 5071–5074. https://doi.org/10.1016/j.bmcl.2008.07.119

Hanwell, M. D., Curtis, D. E., Lonie, D. C., Vandermeersch, T., Zurek, E., & Hutchison, G. R. (2012). Avogadro: An advanced semantic chemical editor, visualization, and analysis platform. *Journal of Cheminformatics*, *4*(1), 17. https://doi.org/10.1186/1758-2946-4-17

Harding, S. D., Sharman, J. L., Faccenda, E., Southan, C., Pawson, A. J., Ireland, S., ... NC-IUPHAR. (2018). The IUPHAR/BPS guide to pharmacology in 2018: Updates and expansion to encompass the new guide to immunopharmacology. *Nucl Acids Res*, *46*, D1091–D1106. https://doi.org/10.1093/nar/gkx1121

Haselmann, H., Röpke, L., Werner, C., Kunze, A., & Geis, C. (2015). Interactions of human autoantibodies with hippocampal GABAergic synaptic transmission—Analyzing antibody-induced effects ex vivo. *Frontiers in Neurology*, *6*, 136.

Hibbs, R. E., & Gouaux, E. (2011). Principles of activation and permeation in an anion-selective Cys-loop receptor. *Nature*, *474*(7349), 54–60. https://doi.org/10.1038/nature10139

Huckvale, R., Mortensen, M., Pryde, D., Smart, T. G., & Baker, J. R. (2016). Azogabazine: A photochromic antagonist of the GABA_A receptor. *Organic & Biomolecular Chemistry*, *14*(28), 6676–6678. https://doi.org/10.1039/c6ob01101b

Humphrey, W., Dalke, A., & Schulten, K. (1996). VMD: Visual molecular dynamics. *Journal of Molecular Graphics*, *14*(1), 33–38. https://doi.org/10.1016/0263-7855(96)00018-5

Johnston, G. A., Chebib, M., Hanrahan, J. R., & Mewett, K. N. (2003). GABA(C) receptors as drug targets. *Current Drug Targets. CNS and Neurological Disorders*, *2*, 260–268. https://doi.org/10.2174/1568007033482805

Kienzler, M. A., Reiner, A., Trautman, E., Yoo, S., Trauner, D., & Isacoff, E. Y. (2013). A red-shifted, fast-relaxing azobenzene photoswitch for visible light control of an ionotropic glutamate receptor. *Journal of the American Chemical Society*, *135*(47), 17683–17686. https://doi.org/10.1021/ja408104w

Kilkenny, C., Browne, W., Cuthill, I. C., Emerson, M., & Altman, D. G. (2010). Animal research: Reporting in vivo experiments: The ARRIVE guidelines. *British Journal of Pharmacology*, *160*, 1577–1579.

Kim, H., Gao, J., & Burgess, D. J. (2009). Evaluation of solvent effects on protonation using NMR spectroscopy: Implication in salt formation. *International Journal of Pharmaceutics*, *377*, 105–111. https://doi.org/10.1016/j.ijpharm.2009.05.018

Korshoej, A. R., Holm, M. M., Jensen, K., & Lambert, J. D. (2010). Kinetic analysis of evoked IPSCs discloses mechanism of antagonism of synaptic GABA_A receptors by picrotoxin. *British Journal of Pharmacology*, *159*(3), 636–649. https://doi.org/10.1111/j.1476-5381.2009.00542.x

Kramer, R. H., Mourot, A., & Adesnik, H. (2013). Optogenetic pharmacology for control of native neuronal signaling proteins. *Nature Neuroscience*, *16*(7), 816–823. https://doi.org/10.1038/nn.3424

Langosch, D., Becker, C. M., & Betz, H. (1990). The inhibitory glycine receptor: A ligand-gated chloride channel of the central nervous system. *European Journal of Biochemistry*, *194*(1), 1–8. https://doi.org/10.1111/j.1432-1033.1990.tb19419.x

Laverty, D., Desai, R., Uchański, T., Masiulis, S., Stec, W. J., Malinauskas, T., ... Aricescu, A. R. (2019). Cryo-EM structure of the human $\alpha_1\beta_3\gamma_2$ GABA$_A$ receptor in a lipid bilayer. *Nature*, *565*(7740), 516–520. https://doi.org/10.1038/s41586-018-0833-4

Laverty, D., Thomas, P., Field, M., Andersen, O. J., Gold, M. G., Biggin, P. C., ... Smart, T. G. (2017). Crystal structures of a GABA$_A$-receptor chimera reveal new endogenous neurosteroid-binding sites. *Nature Structural and Molecular Biology*, *24*(11), 977–985. https://doi.org/10.1038/nsmb.3477

Lin, W. C., Davenport, C. M., Mourot, A., Vytla, D., Smith, C. M., Medeiros, K. A., ... Kramer, R. H. (2014). Engineering a light-regulated GABAA receptor for optical control of neural inhibition. *ACS Chemical Biology*, *9*(7), 1414–1419. https://doi.org/10.1021/cb500167u

Lin, W. C., Tsai, M. C., Davenport, C. M., Smith, C. M., Veit, J., Wilson, N. M., ... Kramer, R. H. (2015). A comprehensive optogenetic pharmacology toolkit for in vivo control of GABA$_A$ receptors and synaptic inhibition. *Neuron*, *88*(5), 879–891. https://doi.org/10.1016/j.neuron.2015.10.026

Lin, W. C., Tsai, M. C., Rajappa, R., & Kramer, R. H. (2018). Design of a highly bistable photoswitchable tethered ligand for rapid and sustained manipulation of neurotransmission. *Journal of the American Chemical Society.*, *140*, 7445–7448. https://doi.org/10.1021/jacs.8b03942

Lynch, J. W. (2004). Molecular structure and function of the glycine receptor chloride channel. *Physiological Reviews*, *84*(4), 1051–1095. https://doi.org/10.1152/physrev.00042.2003

Lynch, J. W., Rajendra, S., Barry, P. H., & Schofield, P. R. (1995). Mutations affecting the glycine receptor agonist transduction mechanism convert the competitive antagonist, picrotoxin, into an allosteric potentiator. *Journal of Biological Chemistry*, *270*(23), 13799–13806. https://doi.org/10.1074/jbc.270.23.13799

Maleeva, G., Peiretti, F., Zhorov, B. S., & Bregestovski, P. (2017). Voltage-dependent inhibition of glycine receptor channels by niflumic acid. *Frontiers in Molecular Neuroscience*, *10*, 125. https://doi.org/10.3389/fnmol.2017.00125

Masiulis, S., Desai, R., Uchański, T., Martin, I. S., Laverty, D., Karia, D., ... Steyaert, J. (2019). GABA$_A$ receptor signalling mechanisms revealed by structural pharmacology. *Nature*, *565*(7740), 454–459. https://doi.org/10.1038/s41586-018-0832-5

Middendorp, S. J., Maldifassi, M. C., Baur, R., & Sigel, E. (2015). Positive modulation of synaptic and extrasynaptic GABA$_A$ receptors by an antagonist of the high affinity benzodiazepine binding site. *Neuropharmacology*, *95*, 459–467. https://doi.org/10.1016/j.neuropharm.2015.04.027

Mukhtarov, M., Liguori, L., Waseem, T., Rocca, F., Buldakova, S., Arosio, D., & Bregestovski, P. (2013). Calibration and functional analysis of three genetically encoded Cl⁻/pH sensors. *Frontiers in Molecular Neuroscience*, *6*, 9. https://doi.org/10.3389/fnmol.2013.00009

Naffaa, M. M., Chebib, M., Hibbs, D. E., & Hanrahan, J. R. (2015). Comparison of templates for homology model of ρ1 GABAC receptors: More insights to the orthosteric binding site's structure and functionality. *Journal of Molecular Graphics and Modelling*, *62*, 43–55. https://doi.org/10.1016/j.jmgm.2015.09.002

Pettersen, E. F., Goddard, T. D., Huang, C. C., Couch, G. S., Greenblatt, D. M., Meng, E. C., & Ferrin, T. E. (2004). UCSF Chimera—A visualization system for exploratory research and analysis. *Journal of Computational Chemistry*, *25*(13), 1605–1612. https://doi.org/10.1002/jcc.20084

Petukhova, E., Ponomareva, D., Mukhamedyarov, M., Maleeva, G., & Bregestovski, P. (2018). Developmental changes in the inhibition of glycinergic synaptic currents by niflumic acid in hypoglossal motoneurons. *Frontiers in Molecular Neuroscience, 11*, 416. https://doi.org/10.3389/fnmol.2018.00416

Priewisch, B., & Rück-Braun, K. (2005). Efficient preparation of nitrosoarenes for the synthesis of azobenzenes. *The Journal of Organic Chemistry*, *70*, 2350–2352. https://doi.org/10.1021/jo048544x

Ragozzino, D., Woodward, R. M., Murata, Y., Eusebi, F., Overman, L. E., & Miledi, R. (1996). Design and in vitro pharmacology of a selective γ-aminobutyric acid C receptor antagonist. *Molecular Pharmacology*, *50*(4), 1024–1030.

Rajagopal, A. K., & Callaway, J. (1973). Inhomogeneous electron gas. *Physical Review B*, *7*(5), 1912–1919. https://doi.org/10.1103/PhysRevB.7.1912

Raju, S. G., Barber, A. F., LeBard, D. N., Klein, M. L., & Carnevale, V. (2013). Exploring volatile general anesthetic binding to a closed membrane-bound bacterial voltage-gated sodium channel via computation. *PLoS Computational Biology*, *9*(6), e1003090. https://doi.org/10.1371/journal.pcbi.1003090

Richter, L., De Graaf, C., Sieghart, W., Varagic, Z., Mörzinger, M., De Esch, I. J., ... Ernst, M. (2012). Diazepam-bound GABA$_A$ receptor models identify new benzodiazepine binding-site ligands. *Nature Chemical Biology*, *8*(5), 455–464. https://doi.org/10.1038/nchembio.917

Rundström, N., Schmieden, V., Betz, H., Bormann, J., & Langosch, D. (1994). Cyanotriphenylborate: Subtype-specific blocker of glycine receptor chloride channels. *Proceedings of the National Academy of Sciences*, *91*(19), 8950–8954. https://doi.org/10.1073/pnas.91.19.8950

Severino, S., Fiorino, F., Perissutti, E., Fresentese, F., Cirino, G., Roviezzo, F., ... Caliendo, G. (2008). Synthesis and pharmacological evaluation of peptide-mimetic protease-activated receptor-1 antagonists containing novel heterocyclic scaffolds. *Bioorganic & Medicinal Chemistry*, *16*, 6009–6020. https://doi.org/10.1016/j.bmc.2008.04.059

Sieghart, W. (2015). Allosteric modulation of GABA$_A$ receptors via multiple drug-binding sites. *Advances in Pharmacology*, *72*, 53–96. https://doi.org/10.1016/bs.apha.2014.10.002

Sieghart, W., & Sperk, G. (2002). Subunit composition, distribution and function of GABA$_A$ receptor subtypes. *Current Topics in Medicinal Chemistry*, *2*, 795–816. https://doi.org/10.2174/1568026023393507

Stein, M., Middendorp, S. J., Carta, V., Pejo, E., Raines, D. E., Forman, S. A., ... Trauner, D. (2012). Azo-propofols: Photochromic potentiators of GABA$_A$ receptors. *Angewandte Chemie International Edition*, *51*(42), 10500–10504. https://doi.org/10.1002/anie.201205475

Stephens, P. J., Devlin, F. J., Chabalowski, C. F. N., & Frisch, M. J. (1994). Ab initio calculation of vibrational absorption and circular dichroism spectra using density functional force fields. *The Journal of Physical Chemistry*, *98*(45), 11623–11627. https://doi.org/10.1021/j100096a001

Tan, K. R., Rudolph, U., & Lüscher, C. (2011). Hooked on benzodiazepines: GABA$_A$ receptor subtypes and addiction. *Trends in Neurosciences*, *34*(4), 188–197. https://doi.org/10.1016/j.tins.2011.01.004

Trott, O., & Olson, A. J. (2010). AutoDock Vina: Improving the speed and accuracy of docking with a new scoring function, efficient optimization, and multithreading. *Journal of Computational Chemistry*, *31*(2), 455–461. https://doi.org/10.1002/jcc.21334

Xie, A., Song, X., Ripps, H., & Qian, H. (2008). Cyclothiazide: A subunit-specific inhibitor of GABA$_C$ receptors. *The Journal of Physiology*, *586*(11), 2743–2752. https://doi.org/10.1113/jphysiol.2008.153346

Yu, Y., & Ikeda, T. (2004). Alignment modulation of azobenzene-containing liquid crystal systems by photochemical reactions. *Journal of Photochemistry and Photobiology C: Photochemistry Reviews*, *5*(3), 247–265. https://doi.org/10.1016/j.jphotochemrev.2004.10.004

Yue, L., Pawlowski, M., Dellal, S. S., Xie, A., Feng, F., Otis, T. S., ... Pepperberg, D. R. (2012). Robust photoregulation of GABA$_A$ receptors by allosteric modulation with a propofol analogue. *Nature Communications*, *3*, 1095. https://doi.org/10.1038/ncomms2094

Zhorov, B. S., & Bregestovski, P. D. (2000). Chloride channels of glycine and GABA receptors with blockers: Monte Carlo minimization and structure-activity relationships. *Biophysical Journal*, *78*(4), 1786–1803. https://doi.org/10.1016/S0006-3495(00)76729-4

SUPPORTING INFORMATION

Additional supporting information may be found online in the Supporting Information section at the end of the article.